Journal of Materials Chemistry A

Accepted Manuscript

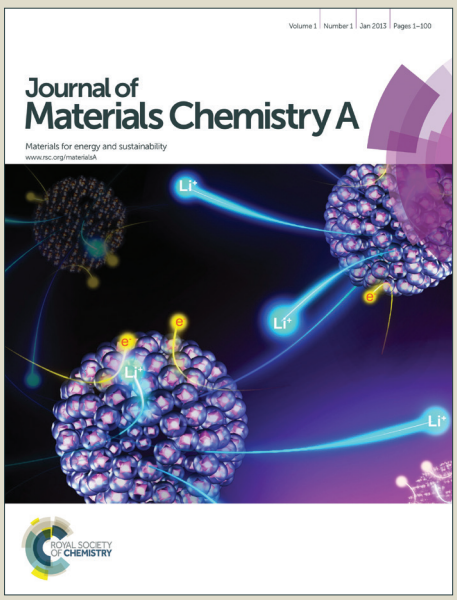

ROYAL SOCIETY OF CHEMISTRY

www.rsc.org/materialsA

Journal Name

RSCPublishing

ARTICLE

Superhydrophobic Surfaces with Near-Zero Sliding Angles Realized from Solvent Relative Permittivity-Mediated Silica Nanoparticle Aggregation

Dae Ho Lee*, Jin Jeong, Se Won Han and Dong Pil Kang

Cite this: DOI: 10.1039/x0xx00000x

Received 00th January 2012,
Accepted 00th January 2012

DOI: 10.1039/x0xx00000x

www.rsc.org/

Multi-scale roughness from nano- to micro-scale over large area is easily generated with a coating of colloidal silica solution in which the silica nanoparticles are aggregated in a controlled manner by the addition of organic solvents. The relative permittivity of the solvent mixture surrounding the silica nanoparticles is shown to be a key factor in the control of nanoparticle aggregation, and can lead to the formation of multi-scale roughness. The coatings are initially superhydrophilic, and become superhydrophobic after surface treatment with typical hydrophobic coupling agents such as octadecyltrichlorosilane. It is shown that there exists a critical value of the relative permittivity of the solvent medium below which coatings with extreme water repellency, along with near-zero sliding angles, are generated.

1. Introduction

Since the first observations of superhydrophobicity in nature in various plants and insects,[1-6] it has become widely accepted that micro- and nano-roughness combined with low surface energy is essential for obtaining artificial superhydrophobic surfaces, and the theoretical understanding of this behavior is based on the Wenzel and Cassie-Baxter models.[7,8] Many papers report the formation of surfaces with multi-scale roughness by various approaches, such as sol-gel processes, physical/chemical vapor deposition, template-based methods, lithography, electro-spinning, and many others, as reviewed recently.[9-11] Multiple complex processing steps, specialized costly reagents and high-tech equipment are often involved in such processes. Compared to the other methods, sol-gel processing is considered attractive due to its simplicity, low cost, and broad applicability.[12-23] Silica nanoparticles synthesized by the Stöber sol-gel process[24] are widely used as the starting material for fabricating superhydrophobic surfaces. The presence of silanol (Si–OH) groups on the surface of the nanoparticles permits subsequent hydrophobization treatment by the addition of traditional coupling agents, such as fluoro-alkyl or alkyl silanes; these are typically applied by post-treatment[19-21] or incorporated during the sol-gel synthesis step.[14-18] It has been recently recognized that the aggregation of silica or polymer nanoparticles is beneficial for superhydrophobicity owing to the formation of micro-roughness. This aggregation effect can be achieved by self-assembly of nanoparticles,[25-27] blending with polymers,[22] using an aggregating agent,[23] coating with multiple layers,[28,29] etc.

From a fundamental standpoint, particle aggregation is a phenomenon related to colloidal stability. Apart from superhydrophobic applications research, the colloidal stability of silica particles in various organic solvents was investigated several decades ago.[30-33] For example, hydrophilic silica particles disperse stably in polar solvents such as ethanol, but they aggregate when non-polar solvents such as cyclohexane are added.[30,31] This behavior is typically understood using the Derjaguin-Landau-Verwey-Overbeek (DLVO) theory,[34,35] *i.e.*, decreased electrostatic repulsion and increased van der Waals (vdW) attraction between colloidal particles in the solvent. In addition, non-DLVO sources of repulsion, such as solvation forces, are also considered, *e.g.*, hydrogen bonding between the solvent molecules and the silica surfaces.[36,37]

In this study, a novel approach to the fabrication of superhydrophobic surfaces is presented which revisits these classical considerations of colloidal stability. Various organic solvents such as chloroform, dichloromethane, toluene, and hexane were added to colloidal silica nanoparticles synthesized using the Stöber process to induce particle aggregation. It is demonstrated that particle aggregation can be controlled by adjusting the relative permittivity of the solvent mixture. Using this simple approach to particle aggregation, nanoparticle coatings with multi-scale roughness and with various dimensions were deposited on glass substrates. Both superhydrophobicity and a near-zero sliding angle were obtained after a subsequent hydrophobization process using a typical coupling agent. Since the focus of this study is on the fabrication of multi-scale surface roughness via nanoparticle aggregation, it will be experimentally demonstrated how the resulting superhydrophobicity is related to the relative permittivity of the solvent, which has not been reported previously to the authors' knowledge.

2. Experimental

Materials

All chemicals—tetraethyl orthosilicate (TEOS, 98%), methyl alcohol (MeOH, ≥99.8%), ethyl alcohol (EtOH ≥99.5%), ammonia solution (28% in H_2O, ≥99.99%), chloroform (Chl, ≥99.5%), dichloromethane (≥99.8%), toluene (99.8%), hexane (>95%), 3-methyl-1-butanol (isopentyl alcohol, IPTA, ≥98.5%), and octadecyltrichlorosilane (ODTS, >90%)—were purchased from Sigma-Aldrich (Yong-in, Korea) and used as received.

Synthesis of silica nanoparticles

TEOS was dissolved in MeOH, and heated to 50 °C in a temperature-controlled shaking incubator. The sol-gel reaction was initiated by adding an aqueous mixture of the ammonia solution and distilled water. The molar concentrations of TEOS and water were 1 and 7.65 M, respectively, and ammonia concentration was adjusted from 0.1 to 0.5 M to control the particle size. The reaction continued until the solid content reached ~7 wt%; only negligible changes were observed afterwards.

Synthesis of acidic silica sol

TEOS was dissolved in MeOH and heated to 50 °C in a temperature-controlled shaking incubator. The sol-gel reaction was initiated by adding an aqueous mixture containing formic acid and distilled water ([TEOS]:[formic acid]:[water]:[MeOH] = 1.5:0.2:4.0:10.9). The reaction continued until the solid content reached ~10 wt%; only negligible changes were observed afterwards.

Preparation of dispersed silica nanoparticles

The silica nanoparticle solutions had pH values of ~10. By the addition of a small amount of formic acid, the pH was adjusted to 4.0. The acidic silica sol was then mixed with the silica nanoparticle solution (silica nanoparticle solution:acidic silica sol = 9:1 based on solid weight). Organic solvents, such as chloroform, dichloromethane, toluene, and hexane, were each added to this solution to induce particle aggregation; these materials will be referred to as "organic-dispersed silica". The added amount of organic solvent was denoted as wt% with respect to total weight of organic-dispersed silica solution.

Film deposition

The organic-dispersed silica materials were coated on glass slides by spin coating (2000 rpm, 20 s) and dried at 300 °C for 1 h. These surfaces were immersed in an octadecyltrichlorosilane (ODTS)/toluene solution (0.5 wt%) for 24 h, washed thoroughly with toluene and ethanol, and dried at 120 °C for 30 min.

Characterization

Particle size was measured using transmission electron microscopy (TEM, JEM2100F, JEOL). Particle size in solution was analyzed by dynamic light scattering (DLS) method (BT-90 Nano Laser Particle Size Analyzer, Bettersize instrument Ltd.). The structure of the coatings was analyzed using optical microscopy (DIMIS, DIMIS-M; Siwon Optical), scanning electron microscopy (SEM, S-4800, HITACHI) and atomic force microscope (AFM, Park systems, XE-100, non-contact mode). The relative permittivity of the mixed solvents used for preparing the organic-dispersed silica were measured using a liquid–dielectric-constant meter (Model 871, NIHON RUFUTO). Hydrophobicity of the coatings following ODTS treatment was characterized using contact-angle measurements (Phoenix 300, SEO).

3. Results and discussion

Silica nanoparticle synthesis

Silica nanoparticles were synthesized according to the typical sol-gel method.[24] Representative TEM images of the resulting nanoparticles with various ammonia concentrations are shown in Fig. 1. Particle size estimates were determined by averaging the diameters as measured using image analysis software (ImageJ, National Institutes of Health); these results are summarized in Fig. 1(f).

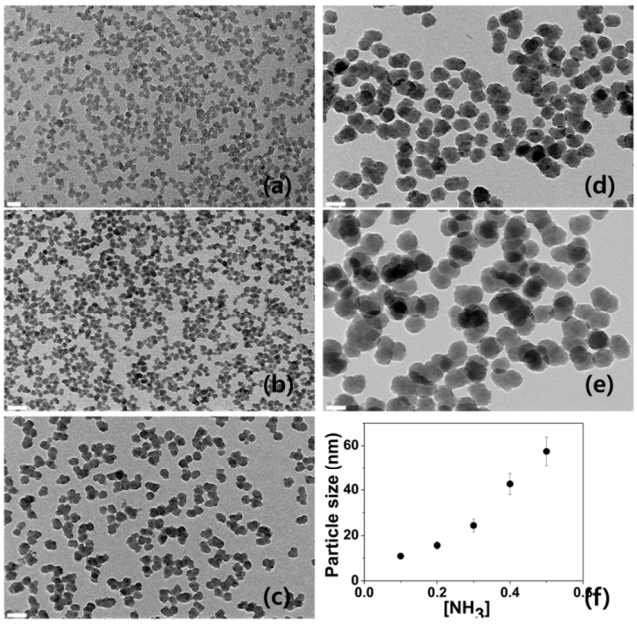

Fig. 1 TEM images of silica nanoparticles synthesized by sol-gel methods at different ammonia concentrations (scale bars : 20 nm for (a), 50 nm for (b) ~ (e)): (a) 0.1 M, (b) 0.2 M, (c) 0.3 M, (d) 0.4 M, and (e) 0.5 M. Average particle diameter values are shown in (f): ~10 nm (a), ~15 nm (b), ~25 nm (c), ~40 nm (d), and ~55 nm (e).

Silica nanoparticles dispersed in mixed organic solvents

As mentioned in Introduction, silica nanoparticles aggregate because of their low colloidal stability in solvents with low polarity.[30-33,36,37] In this study, chloroform, dichloromethane, toluene, and hexane were the solvents used to induce particle aggregation. Additionally, a small amount of the acidic silica sol was added to enhance adhesive strength of the spin-coated layer; the layers deposited without an acidic silica sol addition were too weak to handle for characterization experiments. Since the colloidal stability of silica depends sensitively on the pH,[38] the pH of the silica nanoparticle solution was adjusted to

4 beforehand by adding formic acid; this prevents destabilization due to the pH reduction during mixing of the silica nanoparticle solution (pH ~ 10) with the acidic silica sol.

This nanoparticle/silica sol solution was used as the base, reference solution, and the effect of the addition of organic solvents to this reference solution was systematically investigated. The silica solution became opaque with increasing organic solvent addition. An example of this effect for the addition of chloroform is shown in Fig. 2. These results indicate the formation of domains of increasingly larger size, namely, the size of the silica nanoparticle aggregates. A further increase in the chloroform content above 60 wt% resulted in phase-separation. Hence, chloroform was added only up to 60 wt%.

Fig. 2 Silica nanoparticle (~10 nm) dispersion with increasing chloroform content. The reference sample ("ref") was prepared by mixing silica nanoparticle solution and acidic silica sol (9:1 based on solid weight), and the samples were prepared by adding chloroform to this reference solution in quantities between 15 and 60 wt%.

DLS was used to estimate the aggregated size in the solution. As shown in Fig. 3, the original particle sizes (~12 nm (a), ~67 nm (b)) right after sol-gel process were similar with those observed by TEM (~10 nm and ~40 nm, respectively), and substantially increased with chloroform addition.

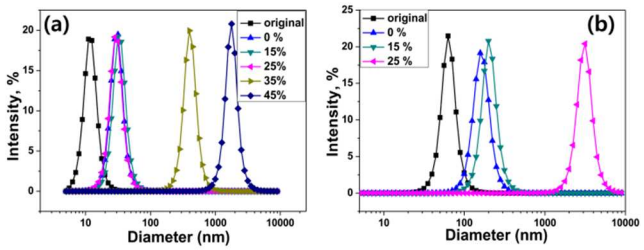

Fig. 3 DLS results for samples of ~10 nm (a) and ~40 nm (b) sizes : the sample "original" denotes as prepared silica nanoparticles by sol-gel process. 0, 15, 25, 35, 45 % denotes the content of chloroform addition after pH adjustment and mixing with acidic silica sol.

In Fig. 3(a), the particle size without chloroform addition (~32 nm, sample "0 %") is slightly higher than the original size (~12 nm) right after sol-gel synthesis. This means slight aggregation occurred during pH adjustment and mixing with acidic silica sol. With addition of chloroform, the particle size substantially increased at 35 wt% (~428 nm), which indicates the particle aggregation becomes significant at this content. At 45 wt%, the aggregated size largely increased to μm level. In Fig. 3(b), the particle size increase is more pronounced. The particle size increases from ~ 67 nm to ~170 nm after pH adjustment and mixing with acidic silica sol. With chloroform addition, the particle size slightly increased at 15 wt% (~214 nm), then, remarkably increased to μm level at 25 wt%. Size analysis was limited above this content due to measurement limit of DLS. Investigation of aggregated size for further increasing chloroform was attempted by in-situ optical microscope observation. For this, a small amount of the silica solution was dropped on a cleaned surface, and quickly observed by optical microscope before drying. Several captured images are shown Fig. 4

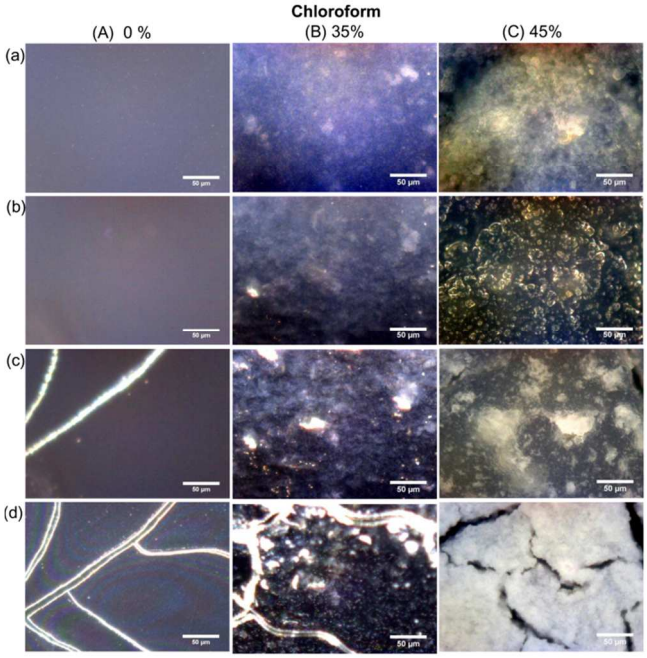

Fig. 4 In-situ optical microscope images of silica nanoparticle (~40 nm in Fig. 1) solutions. Images were captured at time interval of 2 sec (scale bar : 50 μm) : (a) images for solutions right after dropping on substrate; (b), (c) images captured during drying; (d) images after dried. Video files containing all images are provided in Supporting information.

While particles are rarely observed before drying in (A) for no chloroform addition, micro-scale particle shape was distinctly observed in (B) and (C) for 35 and 45 wt% samples, respectively. Furthermore, there was large difference between 35 and 45 wt%. Compared with Fig. 4(B) for 35 wt%, micro-sized aggregates with larger sizes were observed to be much more populated in Fig. 4(C) for 45 wt%. Thus, it can be stated that the silica nanoparticles in solution become largely aggregated in micro-scale at or above 45 wt% chloroform content. Above images also show that surface roughness is more developed when the particle aggregation is sufficient with high chloroform content. It is noted that final dried morphologies are different from the spin-coated images in Fig. 5, with larger crack formation possibly due to increased thickness by dropping and slow evaporation.

Surface structures from organic-dispersed silica coatings

Organic-dispersed silica samples were spin coated onto glass substrates. SEM images (Fig. 5) and optical microscope images

(Fig. 6) indicate various scale roughness is evolved with chloroform addition, which looks more noticeable for larger particle sizes.

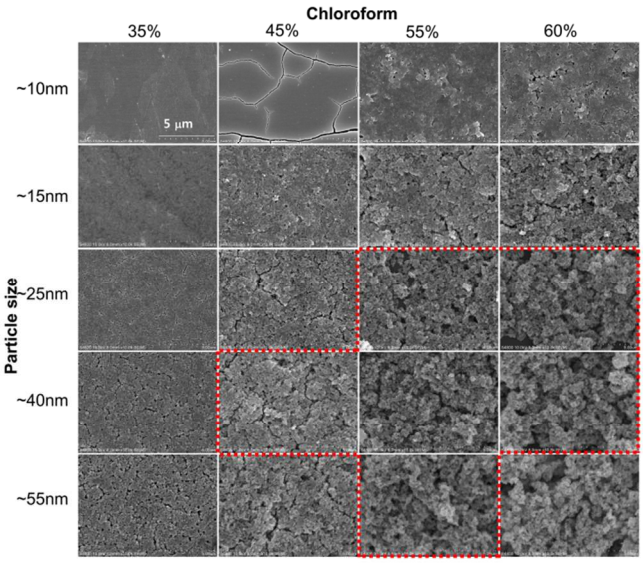

Fig. 5 SEM images of silica-coated substrates (×10k). Images enclosed by the red dotted line correspond to superhydrophobic surfaces with near-zero sliding angles.

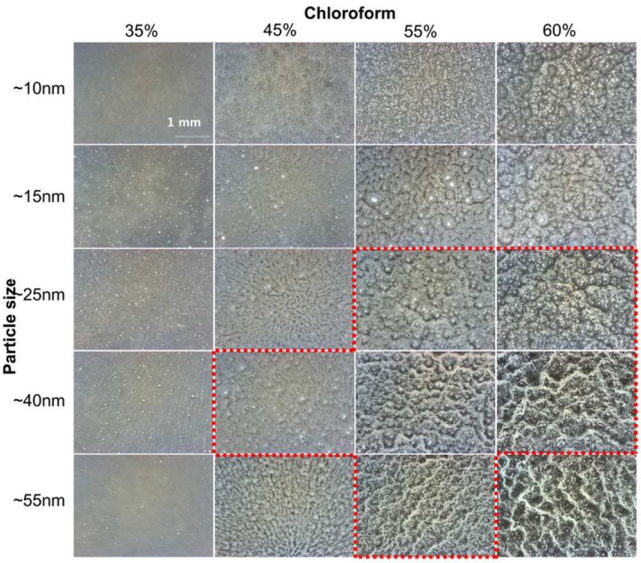

Fig. 6 Optical microscope images (×50) of the samples shown in Fig. 5. The images enclosed by the red dotted line correspond to superhydrophobic surfaces with near-zero sliding angles.

AFM was used to measure the surface roughness. While the increasing roughness was observed with chloroform content and particle size as shown in Fig. S1, the roughness could not be reliably measured for the highly aggregated surfaces with further increasing chloroform content and particle size, due to too much height variation of the sample surfaces and deterioration of AFM tip by silica particles during scanning. In order to elucidate the coating structure of highly aggregated surfaces in more detail, cross-sectional images were obtained in Fig. 7 with several magnifications, *e.g.*, for samples of ~40 nm size with increasing chloroform addition. As shown in Fig. 7, micro-scale roughness begins to emerge from 45 wt% (c), and substantially increases for 55 and 60 wt% (d, e). Roughness scale is observed to be approximately 1 ~ 5 μm, occasionally larger scale with ~ 10 μm, for these high chloroform contents. In addition to micro-scale roughness, nano-scale roughness from silica nanoparticle is also observed in high magnification images (right column). As marked by dot circles, aggregation of several silica nanoparticles composes additional larger nano-scale roughness, which is more distinguishable for high chloroform contents. Thus, it can be stated that multi-scale roughness from nano- to micro-scale exists for aggregated surfaces with high chloroform content, which is responsible for superhydrophobicity, as will be discussed next.

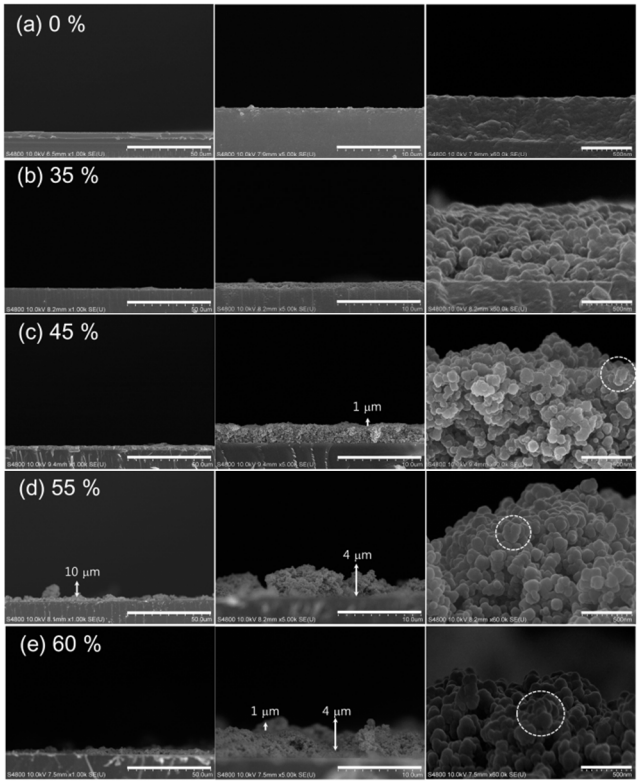

Fig. 7 Cross-sectional SEM images with several magnifications for samples having ~40 nm size with different chloroform content: (a) 0, (b) 35, (c) 45, (d) 55, and (e) 60 wt%. Scale bars are 50 μm (left), 10 μm (middle), and 500 nm (right) .

It is noted that the condition for the micro-scale roughness formation in coatings corresponds to the largely aggregated state in solutions, *i.e.*, 45 wt% chloroform content (Fig. 4c). Though micro-sized aggregates in solution were also observed for 35 wt% (Fig. 4b), only nano-scale roughness is observed with insignificant micro-scale roughness for this case (Fig. 7b). This may be due to merging and overlapping of each aggregated domains during coating and drying. Further aggregation may be required to generate significant micro-scale roughness, which is observed to be 45 wt% in this study.

As shown in Fig. 5 and 6, multi-scale roughness appeared to be more prominent for larger particle size. To verify the roughness formation behaviour according to particle size, cross-sectional images of different particle sizes were compared for samples with high chloroform content (55 wt%).

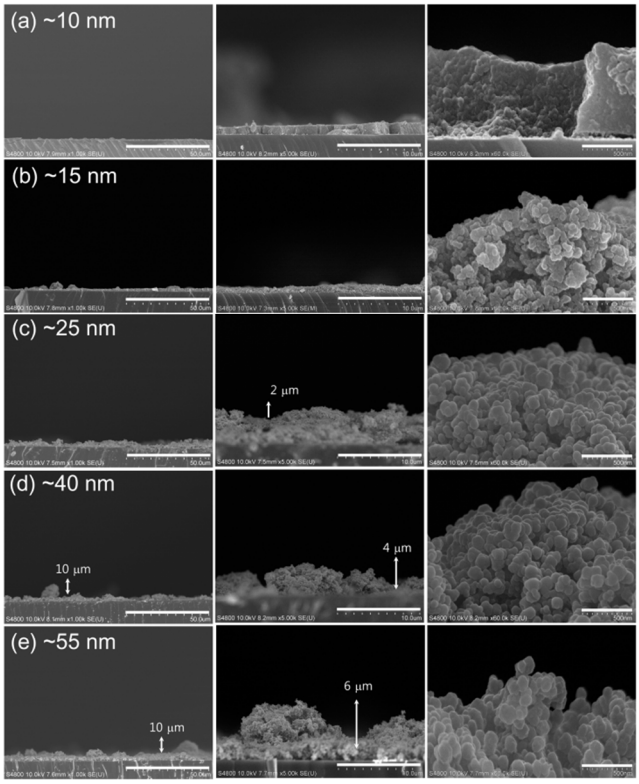

Fig. 8 Cross-sectional SEM images obtained from high chloroform content (55 wt%) solutions : (a) ~10, (b) ~14, (c) ~25, (d) ~40, and (e) ~55 nm. Scale bars are same with those used in Fig. 7.

It is evident from Fig. 8 that larger particles from ~ 25 nm (c) generate aggregated structure with micro-scale roughness. During the structural change of particle aggregations by coating and drying, aggregates from small particles appear to be more densely packed and does not yield high roughness. Only large particles (>15 nm, in this study) are effective for the formation of high roughness with micro-scale, which consequently lead to superhydrophobic coatings as will be discussed next. The height profile observed in Fig. 7 and 8 were similar along the cross-sectional lines, thus, Fig. 6 indicates formation of multi-scale roughness from nano- to micro-scale over large area.

Superhydrophobic surfaces from organic-dispersed silica coating

All the coatings in Fig. 5 exhibit superhydrophilic properties, which can be explained by the multi-scale roughness of the hydrophilic silica surfaces. After treatment with ODTS, hydrophobicity manifested in the coatings and showed remarkable differences depending on the degree of the surface roughness. Fig. 9 shows the water–contact-angle (WCA) values for the samples in Fig. 5. Sliding angle values for corresponding samples are also shown. The WCA values abruptly increase at or above 45 wt% chloroform addition, regardless of the particle size. It is worth noting that superhydrophobicity is obtained for coatings with larger particle sizes, starting from ~25 nm. This is in perfect agreement with the surface morphologies in Fig. 5~8; multi-scale roughness begins to develop at or above 45 wt% chloroform addition, which is prominent for larger particles. Many of these samples, highlighted by the red dotted line in Fig. 5 exhibit extreme water repellency with near-zero sliding angle. Small water droplet was not able to be located on the sample surface due to lower adhesion of water droplet with the sample surface than the needle surface. As shown in Fig. 10, when the droplet size is sufficiently large (> ~ 10 μl), the water droplet rolls away and disappears from the camera view during measurement. The water droplet usually becomes pinned around sample edges where the silica coating may not be uniform and may contain defects. It is supposed that the actual WCA values are close to 180° over most of the sample area.

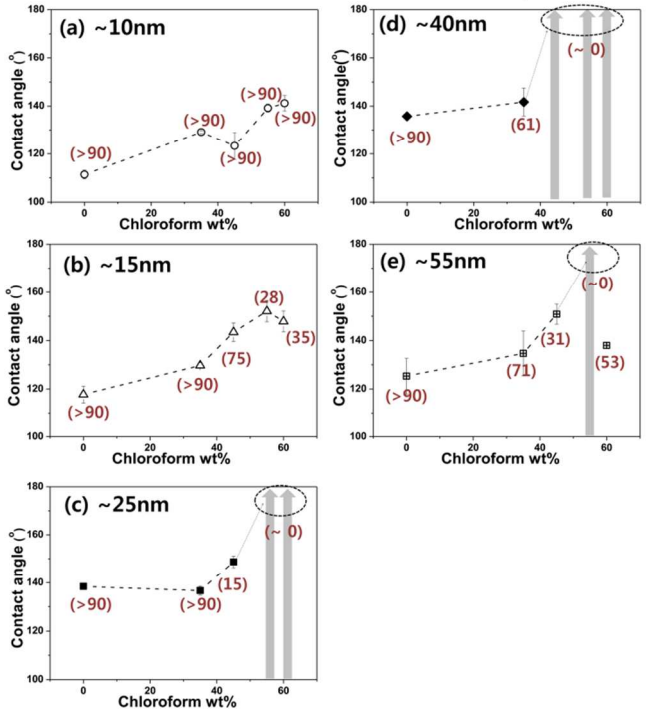

Fig. 9 WCA values for samples shown in Fig. 5 and 6 after the treatment with ODTS. Numbers in brackets are sliding angle values of corresponding samples. The WCA values indicated by the dotted circles were difficult to measure due to the sliding of water droplet on the sample surface (i.e., they possess a near-zero sliding angle). The actual WCA for these coatings is supposed to be close to 180°, as indicated by the arrows.

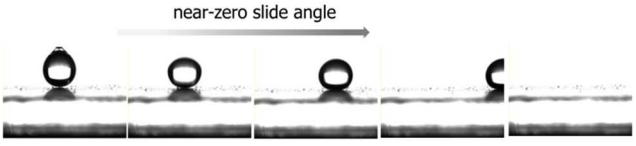

Fig. 10 Representative images showing the extreme water repellency and near-zero sliding angle for the samples whose properties are shown in Fig. 9 and highlighted by the dotted circles. These images describe the behavior of the sample corresponding to particle diameter of ~40 nm aggregated with 55 wt% chloroform. The original video files are provided in the Supporting Information.

For 60 wt% chloroform with ~55 nm size, even larger aggregates are more significantly formed, and pinning of water droplet around these aggregates may decrease WCA for this sample (Fig. S2, Supporting information).

Relative permittivity analysis for solvent media

Silica aggregation in low-polarity organic solvents has been reported earlier.[30-33,36,37] Zeta-potential reduction and changes in the Hamaker constant for silica particles surrounded by organic solvents were analyzed for the DLVO-theory–based explanation, i.e., changes in electrostatic repulsion and vdW attraction between silica particles.[30-33] Non-DLVO repulsion, such as that produced by solvation forces, was also investigated: while polar solvents stabilize silica dispersion (via strong hydrogen bonding to silanol groups on silica surface), low-polarity solvents bring about destabilization and gelation of silica particles (via hydrogen bonding between adjacent silica particles).[36,37]

The relative permittivity (ε) of the solvent is a common measure of solvent polarity. The ε value of a medium-solvent mixture is decreased, *i.e.*, the medium-solvent mixture becomes less polar, by the addition of solvents with low ε values. The polarity of the mixture could eventually decrease to such a degree that it is no longer sufficient for sustaining the dispersion of the polar silica nanoparticles, leading to particle aggregation. Thus, increased aggregation of silica nanoparticles is expected as the relative permittivity of the solvent decreases.

In the previous subsection, it was shown that the WCA values abruptly increased at or above 45 wt% chloroform addition, concomitant with the development of multi-scale roughness. Chloroform is much less polar (ε = 4.8) than the solvents used in silica synthesis: methanol (ε = 32.6), water (ε = 78.4), and ethanol (ε = 24.6, generated during TEOS reaction), thus the relative permittivity of the silica nanoparticle solution decreases with the addition of chloroform.

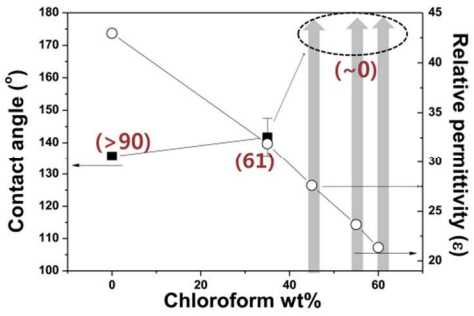

Fig. 11 Relative permittivity of mixed solvents (methanol, water, ethanol, and chloroform) that have the same composition as the medium surrounding the silica nanoparticles. WCA values for 40-nm particle-size coatings are included for comparison.

Fig. 11 shows the ε values of the solvents with different chloroform content superimposed on the WCA data for the resulting coatings. For this analysis, methanol, ethanol, water, and chloroform were mixed in order to make the same composition as the medium surrounding the silica nanoparticles in Fig. 2. Here, a water consumption of 2 mol and an ethanol generation of 4 mol per 1 mol of TEOS during the silica synthesis were taken into consideration in determining the makeup of the solvent mixtures, assuming complete hydrolysis and condensation of TEOS into silica.

As shown in Fig. 11, the relative permittivity of the solvents linearly decrease with chloroform content. The critical chloroform content (45 wt%), at which multi-scale roughness and superhydrophobicity appear, corresponds to an ε value of ~27. Note that silica nanoparticles become largely aggregated in solutions with μm level with ε below ~27 (45wt% chloroform), which clarifies multi-scale roughness is related to particle aggregation in the silica solution.

To verify the role of the relative permittivity in the aggregation of the nanoparticles, the same experiment was repeated using other organic solvents. First, dichloromethane, with a slightly higher relative permittivity (ε = 8.9) than chloroform, was tested using silica nanoparticles of ~40 nm in size. After following the same procedure described above, WCA values for the coated surfaces and ε values of mixed solvents with various dichloromethane contents were analyzed and plotted in Fig. 12.

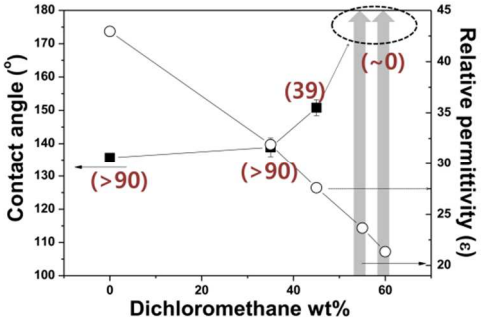

Fig. 12 WCA (filled squares) and ε (hollow circles) values for silica nanoparticle coatings/solutions with different dichloromethane content. Numbers in brackets are sliding angle values of corresponding samples. The WCA values enclosed in the dotted circle correspond to coatings with a near-zero sliding angle.

The WCA values substantially increased starting from 45 wt% dichloromethane (ε ≈ 27). Samples processed with 55 and 60 wt% dichloromethane showed extreme water repellency, i.e., a near-zero sliding angle (cf. Fig. 10). Similarly to the previous results obtained using chloroform, the critical condition for superhydrophobicity was reached near ε value of ~27.

To further verify the above results, non-polar solvents with very low relative permittivity, *e.g.*, toluene (ε = 2.4) and hexane (ε = 1.9), were also tested. In this case, only small amounts of toluene could be incorporated due to the phase separation that occurred in the solutions with 20 wt% or more of toluene.

Within the phase separation limit, relative permittivity of mixed solvents did not decrease below 35, and no significant change in WCA was observed (Fig. S3, Supporting information). A similar behavior was also found for the samples with of hexane additions. In order to avoid phase separation of high toluene- or hexane-content solutions, another co-solvent, isopentyl alcohol (IPTA, ε = 16.7), was introduced. Fig. 13a shows the WCA and ε values for the toluene-based samples with the IPTA content fixed at 30 wt% (with respect to the silica nanoparticle solution before toluene addition). In this case, no phase separation was observed below 45 wt% toluene (Fig. 13c). Additionally, an abrupt increase in WCA was evident, beginning at 25 wt% toluene, together with superhydrophobicity and a near-zero sliding angle. It is interesting to note that the corresponding relative permittivity is 25~30, which is in the same range with the cases in which chloroform and dichloromethane have been used.

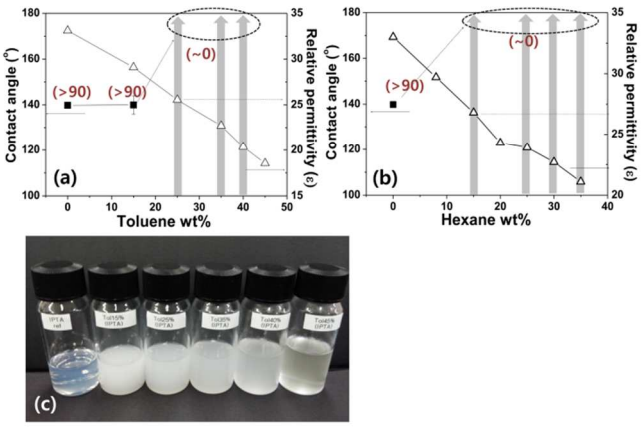

Fig. 13 WCA and ε values of the samples containing IPTA along with (a) toluene and (b) hexane. Numbers in brackets are sliding angle values of corresponding samples. The values in the dotted circles are for measurements on superhydrophobic surfaces with near-zero sliding angles. These solutions were not phase-separated until 45 wt% toluene, as shown in (c).

Samples containing hexane exhibit similar behavior, as seen in Fig. 13b. A substantial increase in WCA was observed starting from 15 wt% hexane, which corresponds to ε ≈27. Below that value, coatings exhibited superhydrophobic behavior with near-zero sliding angles.

All of the data shown in Fig. 11–13 strongly indicate the existence of a critical range of relative permittivity below which substantial increase in WCA was observed. This critical value of the relative permittivity exists in a relatively narrow range of 25~30, regardless of the solvent type or concentration. From the observation that the multi-scale roughness of the coated surfaces and the aggregation of silica nanoparticles in solutions become more prominent with decreasing solvent ε, it can be concluded that significant particle aggregation below a certain ε value plays an important role in the formation of multi-scale roughness and, consequently, of superhydrophobic surfaces, as schematically illustrated in Fig. 14.

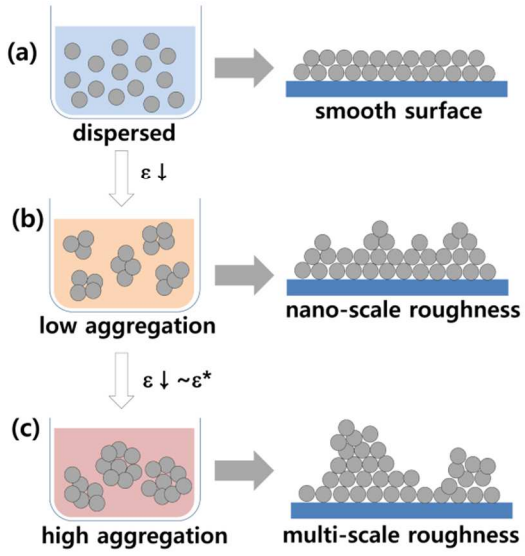

Fig. 14 Simplified schematic illustration expected for development of multi-scale roughness from an aggregated silica solution.

As illustrated with simplified schematics, dispersed particle solution results in a smooth surface (a). As the solvent relative permittivity decreases with addition of organic solvent having low ε, silica nanoparticles become significantly aggregated. But this condition is not sufficient for micro-scale roughness formation. Only nano-scale roughness is formed after coating and drying, which is referred to as *low aggregation* state (b). This condition corresponds to, *e.g.*, 35 wt% chloroform. More substantial particle aggregation is induced by further decreasing ε, leading to micro-scale roughness after coating and drying, which is referred to as *high aggregation* state (c). Chloroform contents from 45 wt% correspond to this condition. Therefore, critical ε for preparation of multi-scale roughness and consequently superhydrophobic surface needs to be designed with rather higher value than theoretically expected one that usually describes the critical condition for initiation of particle aggregation in solution.

Despite the huge number of reports on superhydrophobicity in the literature, sliding angles approaching zero have been rarely obtained.[39,40] In this study, near-zero sliding angle surfaces were fabricated by simple process of particle aggregation followed by surface hydrophobization with non-fluoroalkylsilane (ODTS). In addition to the relative permittivity as a key factor for controlling particle aggregation and facilitating the formation of nano/micro-scale roughness, the initial particle size is also important for realizing superhydrophobic surfaces (cf. Fig. 9). It was observed that larger particles can induce micro-sized aggregates in solution more easily (Fig. 3, 4), and generate more aggregated structure with micro-scale (Fig. 8). That is, producing nano-scale roughness in a proper range (*e.g.*, with particles larger than ~15 nm, as in this study) should be considered together.

The critical value of the relative permittivity may change depending on the types of particles and electrolytes in the solutions since the surface potential and electric double-layer formation around the particles are affected as anticipated by DLVO theory.[34,35] An extended investigation of these factors may lead to a more general explanation of our findings, and this is currently under study.

4. Conclusions

The aggregation of silica nanoparticles was controlled by the addition of organic solvents, such as chloroform or dichloromethane. By increasing the concentration of the solvent, multi-scale roughness was obtained, along with superhydrophobic properties after surface hydrophobization using ODTS. When using non-polar solvents, such as toluene and hexane, this strategy failed at the high concentrations required due to phase separation. When a solvent with an intermediate ε value, such as isopentyl alcohol, was added, the concentration of non-polar solvent could be increased while avoiding phase separation. In addition, it was experimentally demonstrated that the relative permittivity of the solvent surrounding the silica nanoparticles plays a critical role in particle aggregation and the formation of surfaces with multi-scale roughness, regardless of the solvent type. This critical value of the relative permittivity is found to be 25~30 in this study. Below this value, multi-scale roughness and, consequently, superhydrophobicity is obtained. This multi-scale roughness with nano/micro-scale was formed over large area and after hydrophobization using ODTS, these surfaces exhibited extreme water repellency with a near-zero sliding angle. This study presented a simple methodology for preparing superhydrophobic surfaces based on the depositions and control of particle aggregates via modulation of the relative permittivity of the solvent.

Notes and references

* Nano Hybrid Technology Research Centre, Korea Electrotechnology Research Institute, Changwon, Korea. E-mail: neokatari@keri.re.kr; Fax: +82-55-280-1590; Tel: +82-55-280-1688.

Electronic Supplementary Information (ESI) available: Original viedo files are provided showing superhydrophobic surfaces with near-zero sliding angle. See DOI: 10.1039/b000000x/

1 B. Bhushan and Y. C. Jung, *Prog. Mater. Sci.*, 2011, **56**, 1
2 T. Wagner, C. Neinhuis and W. Barthlott, *Acta Zoologica*, 1996, **77**, 213.
3 W. Barthlott and C. Neinhuis, *Planta*, 1997, **202**, 1.
4 A. R. Parker and C. R. Lawrence, *Nature*, 2001, **414**, 33.
5 X. Gao and L. Jiang, *Nature*, 2004, **432**, 36.
6 D. Byun, J. Hong, Saputra, J. H. Ko, Y. J. Lee, H. C. Park, B. K. Byun and J. R. Lukes, *J. Bionic Eng.*, 2009, **6**, 63.
7 R. N. Wenzel, *Ind. Eng. Chem.*, 1936, **28**, 988; A. B. D. Cassie and S. Baxter, *T. Faraday Soc.*, 1944, **40**, 546.
8 W. Choi, A. Tuteja, J. M. Mabry, R. E. Cohen and G. H. McKinley, *J. Colloid Interf. Sci.*, 2009, **339**, 208; J. Bico, U. Thiele and D. Quéré, *Colloid Surface A*, 2002, **206**, 41.
9 P. Roach, N. J. Shirtcliffe and M. I. Newton, *Soft Matter*, 2008, **4**, 224.
10 S. S. Latte, A. B. Gurav, C. S. Maruti, R. S. Vhatkar, *Journal of Surface Engineered Materials and Advanced Technology*, 2012, **2**, 76.
11 E. Celia, T. Darmanin, E. T. de Givenchy, S. Amigoni, F. Guittard, *J. Colloid Interf. Sci.*, 2013, **402**, 1.
12 S. S. Latthe, C. Terashima, K. Nakata, M. Sakaib and A. Fujishima, *J. Mater. Chem. A*, 2014, **2**, 5548-5553
13 L. Wu, J. Hu and J. Zhang, *J. Mater. Chem. A*, 2013, **1**, 14471.
14 S. S. Latthe, H. Imai, V. Ganesan and A. V. Rao, *Appl. Surf. Sci.*, 2009, **256**, 217.
15 E. Kim, J. Kim, S. Kim, *J. Solid Sate Chem.*, 2013, **197**, 23.
16 B. J. Basu, V. Hariprakash, S. T. Aruna, R. V. Lakshmi, J. Manasa and B. S. Shruthi, *J. Sol-Gel Sci. Techn.*, 2010, **56**, 278.
17 Y. H. Xiu, D. W. Hess and C. R. Wong, *J. Colloid Interf. Sci.*, 2008, **326**, 465.
18 H. X. Wang, J. Fang, T. Cheng, J. Ding, L. T. Qu, L. M. Dai, X. G. Wang and T. Lin, *Chem. Commun.*, 2008, No. 7, 877.
19 Q. W. Gan, Q. Zhu, Y. L. Guo and C. Q. Yang, *Ind. Eng. Chem. Res.*, 2009, **48**, 9797.
20 H. Ogihara, J. Xie, and T. Saji, *Colloid Surface A*, 2013, **434**, 35.
21 Y. Xiu, F. Xiao, D. W. Hess and C. P. Wong, *Thin Solid Films*, 2009, **517**, 1610.
22 R.V. Lakshmi, T. Bharathidasan, P. Bera, B. J. Basu, *Surf. Coat. Tech.*, 2012, **206**, 3888.
23 Q. F. Xu, J. N. Wang, and K. D. Sanderson, *ACS Nano*, 2010, **4**, 2201.
24 W. Stöber, A. Fink and E. Bohn, *J. Colloid Interf. Sci.*, 1968, **26**, 62.
25 P. S. Tsai, Y. M. Yang and Y. L. Lee, *Langmuir*, 2006, **22**, 5660.
26 J. Y. Shiu, C. W. Kuo, P. L. Chen and C. Y. Mou, *Chem. Mater.*, 2004, **16**, 561.
27 J. X. Wang, Y. Q. Wen, J. P. Hu, Y. L. Song and L. Jiang, *Adv. Funct. Mater.*, 2007, **17**, 219; I. Flores-Vivian, V. Hejazi, M. I. Kozhukhova, M. Nosonovsky and K. Sobolev, *ACS Appl. Mater. Interfaces*, **2013**, 5, 13284; H. Yang, X Dou, Y. Fang and P. Jiang, *J. Colloid Interf. Sci.*, 2013, **405**, 51.
28 L. Zhai, F. C. Cebeci, R. E. Cohen and M. F. Rubner, *Nano Lett.*, 2004, **4**, 1349.
29 L. Zhang, H. Chen, J. Sunand J. Shen, *Chem. Mater.*, 2007, **19**, 948; H. Tian, T. Yang and Y. Chen, *Thin Solid Films*, 2010, 518, 5183; X. Zhang, F. Shi, X. Yu, H. Liu, Y. Fu, Z. Wang, L. Jiang and X. Li, *J. Am. Chem. Soc. communications*, 2014, **126**, 3064.
30 B. Vincent, Z. Király, S. Emmentt, A. Beaver, *Colloid Surface.*,1990, **49**, 121.
31 Z. Király, L. Turi, I. Dékány, K. Bean, B. Vincent, *Colloid Polym. Sci.*, 1996, **274**, 779.
32 H.A. Ketelson, R. Pelton, M. A. Brook, *Langmuir*, 1996, **12**, 1134.
33 R. Banitez, S. Contreras, J. Goldfarb, *J. Colloid Interf. Sci.*, 1971, **36**, 146.
34 B. V. Derjaguin, L. Landau, *Acta Physicochim. URS.*, 1941, **14**, 633.
35 E.J.W. Verway and J.Th.G.Overbeek, *Theory of the Stability of Lyphobic Colloids*, 1948, Elsevier, Amsterdam.
36 S. R. Raghavan, H.J. Walls, and S. A. Khan, *Langmuir*, 2000, **16**, 7920.
37 H. Barthel, L. Rosch, J. Weis, *Organosilicon chemistry II: From Molecues to material*; N. Auner, J. Weis Eds., VCH Publishers: Weinheim, 1996, 761-777.
38 R.K. Iler, *The Chemistry of Silica*, 1979, Wiley, New York.
39 S. Choi, K.Suh and H. Lee, *Nanotechnology*, 2008, **19**, 275305.
40 L. Gao and T. J. McCarthy, *J. Am. Chem. Soc. communications*, 2006, **128**, 9052; H. K. Park, S. W. Yoon, W. W. Chung, B. K. Min and Y. R. Do, *J. Mater. Chem. A.*, 2013, **1**, 5860.